

# **Journal of Engineering**

journal homepage: www.jcoeng.edu.iq

Volume 31 Number 12 December 2025



# Experimental Evaluation of Free-Fall Gravity Drainage in Water-Drive Reservoirs: Impact of Aquifer Strength and Reservoir Heterogeneity/Homogeneity

Rufaida T. Ibrahim (1) (2), Dahlia A. Al-Obaidi (1) (2), Watheq J. Al-Mudhafar (1) (2), Dandina N. Rao (1) (3)

<sup>1</sup>Department of Petroleum Engineering, College of Engineering, University of Baghdad, Baghdad, Iraq

<sup>2</sup>Basrah Oil Company, Basrah, Iraq

<sup>3</sup> Louisiana State University, Baton Rouge, LA, USA

#### **ABSTRACT**

 ${f T}$ his study experimentally investigated Free-Fall Gravity Drainage (FFGD) under combination-drive conditions in a two-dimensional Hele-Shaw model representing a waterdrive reservoir. An initially high gravity potential from the oil column enabled early oil drainage before aquifer support became dominant. Three water-drive strengths were tested, demonstrating that a stronger aquifer (1.15 psig) accelerated oil recovery to approximately 75% of the original oil in place (OOIP) within 60 minutes, resulting in a final recovery of 79.5%. However, this was accompanied by rapid water breakthrough after 2.5 minutes and high-water cuts exceeding 90%. In contrast, a weaker aguifer (0.725 psig) stabilized the oilwater contact, delaying water encroachment and maintaining zero water cut throughout 240 minutes, albeit with a lower ultimate recovery of 70.2%. Visual observations confirmed that a stable water crest and oil bank were preserved longer under moderate to weak aquifer pressures, extending the gravity-dominated recovery and reducing water handling requirements. Residual oil saturation was higher under weak aquifer support (27.9%) than stronger water drive (16.8%) due to a loss of gravity potential as the oil column declined and limited aquifer support. A comparative experiment in a heterogeneous system revealed approximately 22% lower ultimate recovery and water breakthrough within 5 minutes, attributed to heterogeneity promoting preferential flow, poor sweep efficiency, and early breakthrough. In contrast, the homogeneous system sustained production with no water breakthrough for 300 minutes. These insights strengthen the understanding of gravity drainage and can help guide enhanced oil recovery strategies in water-drive reservoirs.

**Keywords:** Free-fall gravity drainage (FFGD), Combination drive, Aquifer strength, Oil recovery, Hele-shaw model.

Peer review under the responsibility of University of Baghdad.

https://doi.org/10.31026/j.eng.2025.12.01

This is an open access article under the CC BY 4 license (<a href="http://creativecommons.org/licenses/bv/4.0/">http://creativecommons.org/licenses/bv/4.0/</a>).

Article received: 08/05/2025 Article revised: 21/07/2025 Article accepted: 28/07/2025 Article published: 01/12/2025

<sup>\*</sup>Corresponding author



#### 1. INTRODUCTION

Gravity drainage is a proven recovery technique that leverages gravitational force as the primary driving mechanism (Mello et al., 2009; Al-Obaidi and Al-Jawad, 2020; Hasanzadeh et al., 2021). According to (Lewis, 1942), gravity drainage is "the self-propulsion of oil downward in the reservoir rock." It is considered one of the three natural oil driving mechanisms of petroleum reservoirs, alongside solution-gas and water drive. In simple terms, gravity drainage refers to the downward movement of oil under the influence of gravitational force. At the same time, the lighter displacing phase (typically gas) rises to occupy the pore space created by the produced oil.

In primary recovery, gravity drainage may occur as a result of pressure depletion and subsequent fluid segregation, while in secondary or tertiary phases, it can be assisted by gas injection (Hagoort et al., 1980). Fluid stratification within the reservoir is compelling evidence of the influence of gravitational forces (Muskat, 1949). This gravitational force facilitates the segregation of reservoir fluids into stratified layers based on their densities in the orientation required to re-establish density equilibrium (Sharma, 2005). Although gravity segregation of fluids is likely to exist in all petroleum reservoirs to some extent, in certain reservoirs it may play a significant role in oil production (Ahmed and McKinney, 2004; Zobeidi et al., 2022), such as in thick, high-permeability oil reservoirs and naturally fractured reservoirs (Erfani et al., 2021; Hasanzadeh et al., 2021).

While gravitational forces inherently contain the mechanical energy necessary to drain oil from porous media (Lewis, 1942), the concern lies in how efficiently this energy translates into effective oil displacement. (Dumore and Schols, 1974) reported that gravity drainage can result in an oil residual saturation of as low as 5% in high-permeability sandstone cores. The gravity drainage process in oil reservoirs can occur in two primary forms (Schechter and Guo, 1996; Moghaddam and Rasaei, 2015): Free-Fall gravity Drainage (FFGD) and Forced Gravity Drainage (FGD), also widely known as Gas-Assist Gravity Drainage (GAGD). FFGD is a process that has long been recognized as an effective means of recovering hydrocarbons from oil reservoirs (Dykstra, 1978; Moghaddam and Rasaei, 2015) where oil is displaced solely by gravitational forces without external gas injection. This can be accomplished by controlling the pressure reduction and withdrawal rate so that gravity segregation occurs, followed by counter-current flow of gas and oil. Under ideal conditions, where gravity drainage conditions are favorable, or where producing rates are managed to take the full advantage of the gravitational forces, more than 80% of the Original Oil in Place (OOIP) can be recovered (Ahmed, 2019). After solution gas is liberated due to pressure decline, if this gas is conserved in the reservoir and allowed to migrate upward and form a secondary gas cap rather than flowing to the production well, then the reservoir operates under a combined gas-cap drive and gravity drainage mechanism. As the pressure in the gas cap declines, the expanding gas forms a gas-oil front, displacing oil ahead of it as an oil bank. The gas-oil front continues to advance downward and sideways toward the production well. Recent advances in gravity-stable gas injection methods have made it possible to improve vertical and areal sweep efficiency by supporting stable displacement fronts within the reservoir. GAGD utilizes gravity-stable gas injection for horizontal reservoirs, enhancing volumetric sweeps and improving oil production in secondary and tertiary recovery phases. It has consistently proven through experimental and simulation studies to be a highly efficient recovery method (Paidin, 2006; Mahmoud and Rao, 2007; Sharma and Rao, 2008; Mahmoud and Rao, 2008; Rostami et al., 2010; Rao, 2012; Al-Mudhafar et al., 2018; Dzulkarnain Iskandar, 2018; Al-Tameemi, 2019; Al-Obaidi et al., 2022; Al-



**Obaidi et al., 2024)**. It strategically uses vertical injection wells and horizontal production wells (Jadhawar and Sarma, 2010).

Therefore, a thorough understanding of gravity drainage as a natural recovery mechanism is crucial for improving oil recovery in many reservoirs. As long as fluids are present in a porous medium, gravity will continue to act to redistribute and segregate them according to density differences. This natural energy can be strategically utilized to enhance recovery. Four principal hypotheses guided this experimental study. First, in a gravity-drainage system, oil drains under the influence of gravitational forces acting on the fluid column, with the top of the experimental column exposed to atmospheric pressure, allowing ambient air to enter and permitting free-fall flow. The driving force is expected to be strongest initially, as the height of the saturated oil column is at its maximum at the beginning of production. Second, placing a horizontal well near the base of the pay zone will reduce flow resistance and enhance drainage efficiency (Joshi, 1991). This configuration also allows for improved recovery, as the well location helps maintain a stronger pressure gradient due to the higher oil column height, supporting sustained oil production (Alamooti and Malekabadi, 2018). Third, it is hypothesized that increasing the strength of the water drive will accelerate early oil recovery but may also promote earlier water breakthrough, thereby diminishing recovery efficiency over longer time frames. Finally, homogeneous porous media are anticipated to achieve higher ultimate oil recovery and a lower water cut under FFGD conditions in a water-drive reservoir than heterogeneous porous media. This is attributed to a more stable displacement front and reduced channeling, which enhances sweep efficiency and delays water breakthrough.

Although gravity drainage has long been recognized, its performance as part of a combination drive in water-drive reservoirs has not been systematically evaluated, particularly about aquifer strength and reservoir heterogeneity. This raises important questions about how FFGD interacts with water drive to affect oil recovery and water production.

Therefore, this study aims to investigate the role of gravity drainage in a water-drive reservoir through a series of controlled FFGD experiments performed in a two-dimensional (2D) Hele-Shaw model. The focus is on understanding how varying aquifer strengths influence recovery performance and water encroachment behavior in a homogeneous porous medium, while also addressing the challenges posed by reservoir heterogeneity by comparing findings from the literature on heterogeneous systems. The experimental setup and protocols were designed to provide reproducible and clear observations of the displacement process using dyed fluids and high-resolution imaging. This investigation also serves as a benchmark for future GAGD studies, where controlled gas injection could improve recovery performance and mitigate water encroachment.

# 2. EXPERIMENTAL SETUP AND METHODOLOGY

#### 2.1 Experimental Workflow

**Fig. 1** summarizes the general workflow adopted in this study, from model preparation and characterization to data analysis. This approach ensures consistent, reproducible runs and reliable recovery factor and water cut evaluation.



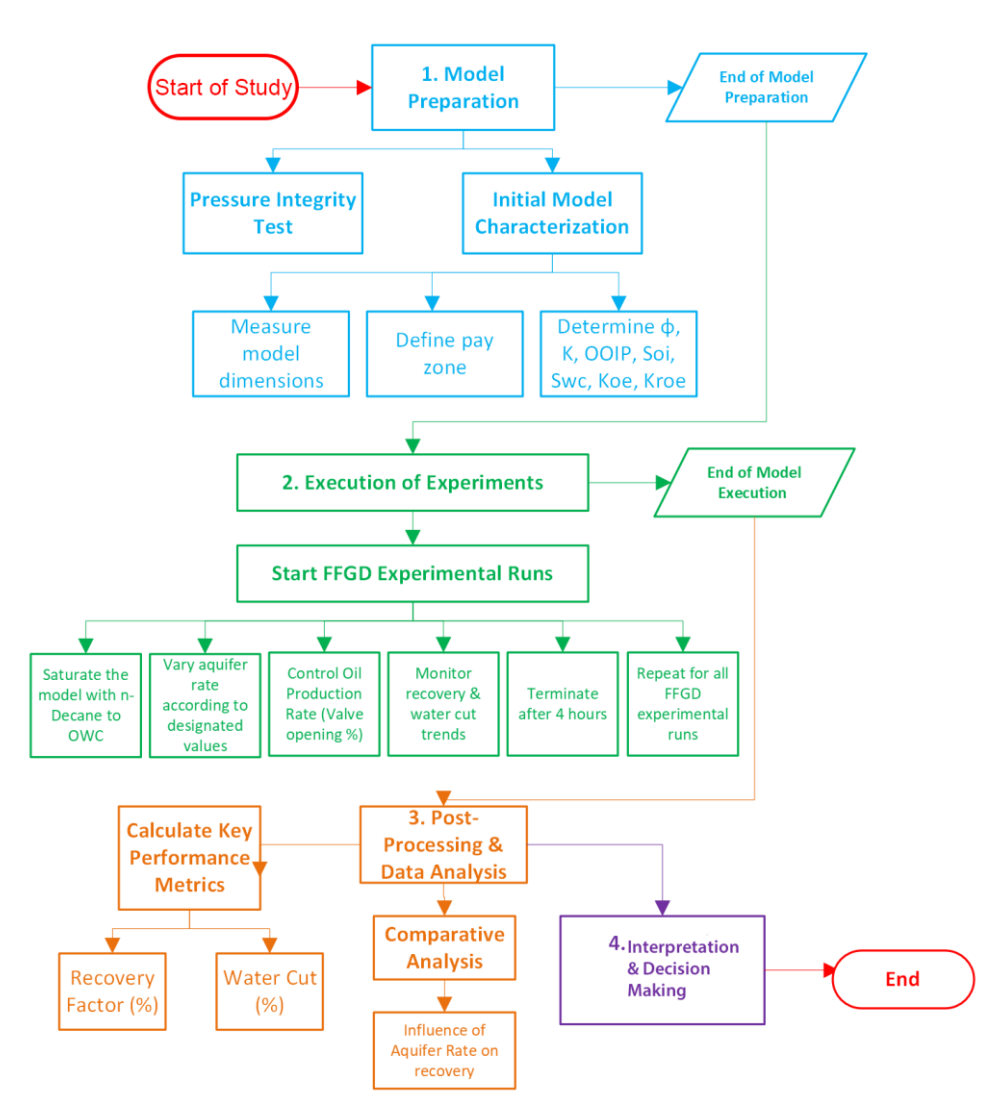


**Figure 1**. Flowchart summarizing the experimental methodology adopted in this study.

#### 2.2 Material Used

To simulate the oleic and aqueous phases in the FFGD process in a water-drive reservoir, n-Decane, a non-polar alkane hydrocarbon ( $C_{10}H_{22}$ ) ( $\geq 99\%$  purity, CAS 124-18-5, product number 8.03405.1000, Merck KGaA, Darmstadt, Germany) was used as the oil phase due to its immiscibility with water and its capacity to represent typical hydrocarbon behavior. The negative spreading coefficient (Sow<0) prevented the substance from spreading across the water phase, enabling clear observations of the two phases. Deionized Water (DIW), sourced from Al-Ameer Distilled Water Factory, Baghdad, Iraq, was used as the aqueous phase.

To visualize fluid flow phenomena, Sudan II ( $C_{18}H_{16}N_{20}$ ), a fat-soluble dye with a density of 1.14 g/cm<sup>3</sup>, was added to n-Decane, while a blue food-grade dye was added to water. The physical properties of the test fluids are presented in **Table 1**, and their relevant interfacial tensions (IFT) and calculated spreading coefficient are summarized in **Table 2**.

Ottawa silica sand ( $SiO_2$ ), characterized by its high purity of 99.01%, specific gravity of 2.65 g/cc, and median particle size (D50) of 0.84 mm, was used to create a homogenous porous medium.



**Table 1.**The physical properties of the fluids used in this study.

Phase	Fluid	Density (g/cm³)	Viscosity (cP)	MW(g/mol)
Aqueous	Deionized Water- Blue dyed	1.05	1.00	18.0153
Oleic	n-Decane- Red dyed	0.73	0.84	142.2817

Table 2. IFT and spreading coefficient of the fluid system (Zhou and Blunt, 1997).

System	σwg (mN/m)	σοw (mN/m)	σog (mN/m)	Sow (mN/m)
Air + n-Decane + Water	72.1	52.0	23.0	-2.9

# 2.3 Sand Packing Procedure

The sand packing procedure followed a dry-packing method adapted from (**Oliviera et al., 1996**). Silica sand was poured into the glass model in controlled increments of 1 cm and uniformly distributed across its width. After each increment, a wooden pestle with a rectangular head was used for gentle manual compaction. Final compaction was achieved by applying low-pressure gas to maintain uniformity in longitudinal and lateral directions, effectively minimizing boundary effects and preventing channeling.

## 2.4 Experimental Apparatus Configuration

The experimental setup consisted of a 2D Hele-Shaw apparatus with a glass model (transparent sand holder), a fluid system, and measurement, data acquisition, and visualization systems. **Fig. 2** illustrates the experimental configuration schematically, and **Fig. 3** presents the complete laboratory setup.

Experiments were conducted using a 2D Hele-Shaw apparatus, designed and constructed by **(Al-Obaidi, 2020)**. The apparatus consisted of an enclosed iron frame with a transparent panel packed with silica sand, representing a reservoir–aquifer system. Four high-strength tempered glass plates, each with a thickness of 10 mm, were used to create the model. These plates were thermally tempered in-house by heating and then rapidly air-quenched. The Hele-Shaw model has internal dimensions of 60 cm (L) × 30.7 cm (W) × 3 cm (D). The frame incorporated inlet and outlet flow systems for injection and production. A horizontal well was simulated within the glass model, located above the oil–water contact (OWC), using a ¼-inch perforated tube produced by a hand drill fitted with a 1/64-inch (400  $\mu$ m) drill bit to ensure uniform and consistently spaced perforations. The tube extended across the model's width.

A graduated beaker with a floating valve supplied water to simulate the water-drive reservoir. The float valve acted as a mechanical liquid-level controller, responding to changes in water surface elevation and maintaining a constant head through a supplementary container. This configuration reduced pressure fluctuations, supporting stable water injection. The water head in the beaker was adjusted between runs using the height-adjustable platform to set the specific water drive pressure being tested. Within each run, however, the water level remained fixed. The same system was also used to saturate the sand pack and pump n-decane during the oil-flooding phases of the experiments.

The measurement system consisted of a weight cell sensor, a graduated cylinder, pressure gauges, and a flowmeter. The cell featured an aluminum load cell element and an integrated signal processor that converted analogue signals to a digital format, transmitting them to a computer via Excel Data Streamer. This provided continuous mass measurement of



produced fluids in the collection cylinder. While the load cell provided high accuracy for single-phase production, it was unable to differentiate between oil and water during two-phase flow; therefore, cumulative production volumes were assessed using camera video recordings and a graduated cylinder. A graduated cylinder with a capacity of 500 cm<sup>3</sup>, measured in 5 cm<sup>3</sup> increments, was used to record the cumulative volume of n-Decane and water over time, evaluating production trends and water cut. Three low-pressure dial-type gauges (OSAKA, Japan, range 0–0.1 MPa, accuracy ±0.002 MPa) were installed at critical points: one in the gas injection line for integrity testing, another in the water injection line to monitor aquifer pressure, and a third connected for oil effective permeability calculations. A float-type variable-area flowmeter (LZB-3WB, Wuxi Kairda Instrument Technology Co., China) was fitted on the water injection line. It visually confirmed the water injection rate during tests and supported permeability measurements.

The experimental runs were recorded using two XVISION-HD cameras (model XV-WH3204P4, 4K Ultra HD resolution, manufactured by XVISION, Hong Kong) to capture real-time visuals of the displacement process. The first camera was positioned to capture the Hele-Shaw model, allowing for qualitative observations of oil bank advancement, water crest development, and the location of the OWC throughout the experiments. The second camera focused on a graduated cylinder, recording the cumulative volumes of produced n-Decane and water as a function of time. The dual-camera configuration ensured precise documentation of the displacement dynamics in the model and the production data.

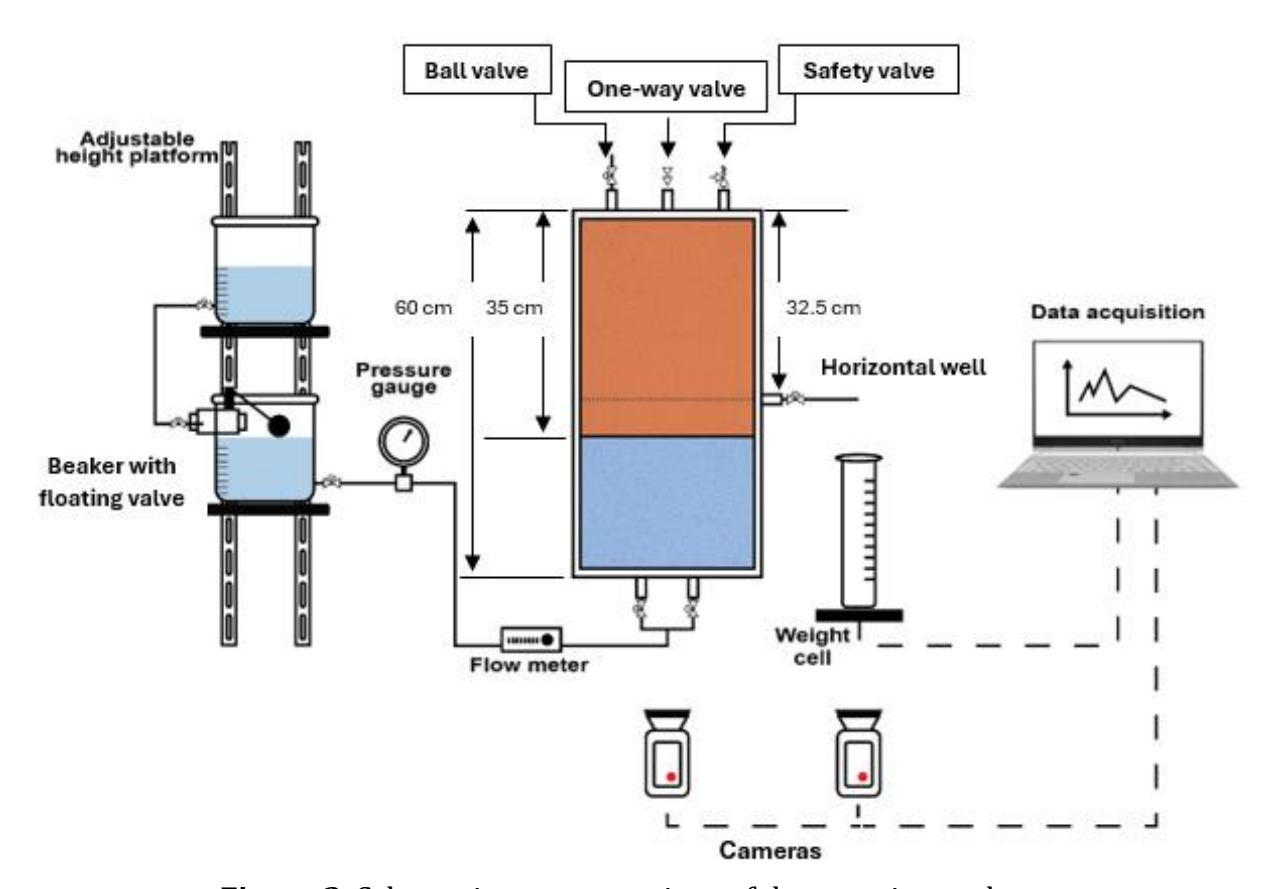


**Figure 2.** Schematic representations of the experimental setup.



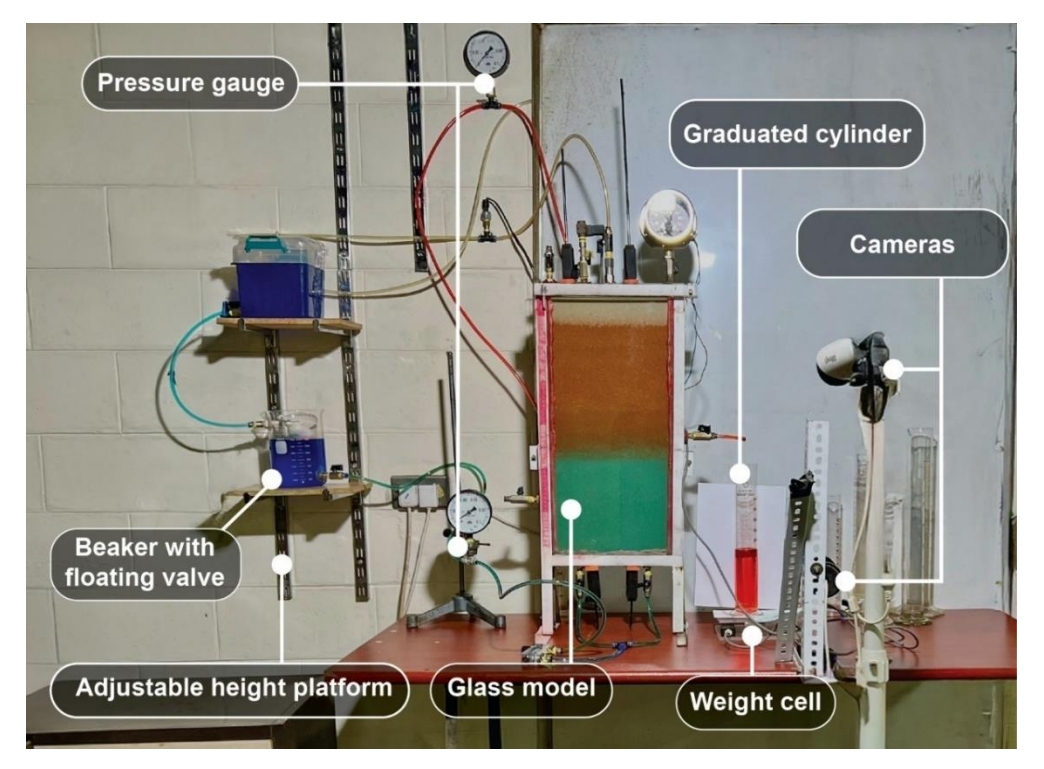


**Figure 3.** Laboratory setup for the FFGD experiments.

# 2.5 Pressure Integrity Test

Before conducting the experiments, a pressure integrity test was performed to ensure the glass model was leak-free. The test was conducted by connecting a  $\rm CO_2$  cylinder to the top inlet of the model through a one-way valve and applying a regulated pressure of 0.0082 MPa (1.19 psig) using the cylinder built-in pressure regulator. The pressure inside the model was monitored with the pressure gauge installed along the gas injection line. Once the internal model pressure equilibrated with the set regulator pressure, gas flow ceased, and the gauge reading was observed for 5 minutes. The pressure remained constant during this time, indicating no observable leaks in the system.

# 2.6 Initial Characterization of the Model

#### 2.6.1 Porosity and Permeability Measurements

The first property evaluated was porosity, calculated as the ratio of the measured pore volume (determined by water saturation) to the bulk volume of the silica pack in the glass model, which was 5440 cm<sup>3</sup>. The medium has a porosity of 32.5%. **Fig. 4a-c** illustrates porosity measurement steps.

Subsequently, the absolute permeability (K) of the silica pack was determined using Darcy equation (Lake et al., 2014) Eq. (1):

$$K_{abs.} = \frac{q u l}{A \Delta p} \tag{1}$$

Where q is the volumetric water flow rate through the packed porous medium,  $\mu$  is the fluid viscosity, L is the flow path length, A is the cross-sectional area, and  $\Delta p$  is the pressure



difference across the porous medium. As illustrated in **Fig. 4d**, water was injected from the bottom of the glass model under constant head conditions, with the top valve connected to a tube open to atmospheric pressure. Because the outlet was atmospheric, the pressure gauge on the injection line directly reflected the applied pressure differential. The water flow rate was monitored using the installed flow meter on the water injection line. Several flow rates were collected by adjusting the water head level to vary the pressure differential **(Amyx et al., 1960; Dake, 1983)**. These data were then plotted, with the normalized pressure gradient  $(A\Delta p/\mu L)$  on the x-axis and the volumetric flow rate q on the y-axis. As shown in **Fig. 5**, a regression line was fitted to these points, where the trend line slope corresponded to the absolute permeability of the homogeneous model, measured at approximately 5.02 Darcy with an  $R^2$  of 0.9915.



**Figure 4**. Porosity and permeability measurement procedure: (a) Base condition - silica-filled Hele-Shaw Model. (b) Partial saturation during water injection. (c) Fully saturated Hele-Shaw model containing 1,771 cm<sup>3</sup> of water. (d) Permeability measurement.

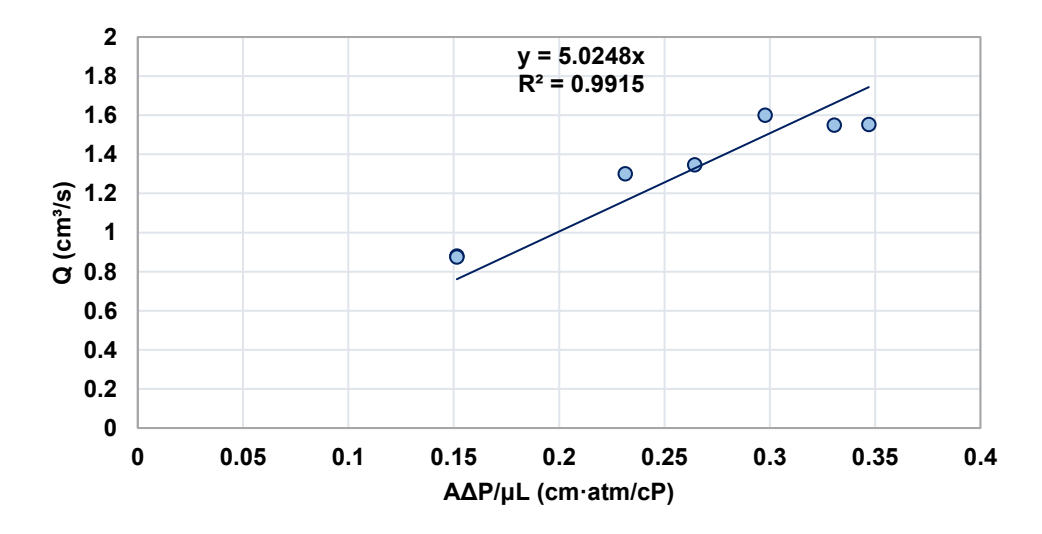


**Figure 5.** The relationship between the normalized pressure gradient and the flow rate of the permeability estimation.



The Carman-Kozeny Eq. (2) **(Kozeny, 1937)** was applied to provide theoretical validation of the measured permeability. K was 4.88 Darcy, consistent with the permeability derived from the experiment.

$$k = \frac{D_p^2 \times \emptyset^3}{72\tau (1-\emptyset)^2}$$
 (2)

Where k is the absolute permeability,  $D_p$  is the average particle diameter,  $\varphi$  is the porosity, and  $\tau$  is the tortuosity factor (measuring the tortuosity of the sand pack is beyond this research scope; therefore, it is set to the typical value of 1.5 for sand packs (**Sharma and Rao, 2008**).

# 2.6.2 Fluid Saturation and Permeability Parameters

Lastly, connate water saturation, oil effective permeability, and endpoint oil relative permeability were obtained. The process was conducted under a controlled, low oil injection rate to ensure a stable and uniform displacement. **Fig. 6** provides a detailed schematic representation of the flow path and injection and production points. All experimental tests were performed at atmospheric pressure and temperature. To measure OOIP and water saturation, the following steps were followed:

- 1. The invaded zone was part of the model occupied by n-Decane, extending from the top of the model to the OWC at a depth of 35cm. The bulk volume of the pay zone  $(VB_{pay\ zone})$  was equal to 3223.5 cm<sup>3</sup>.
- 2. Since one pipe lay within the pay zone, the adjusted bulk volume of the pay zone (silica only) was found by subtracting the pipe's outer volume from the bulk volume of the pay zone, which is adjusted to 3204 cm<sup>3</sup>.
- 3. Original water volume in the pay zone (VP<sub>pay zone</sub>) was found to be 1041 cm<sup>3</sup> using Eq. (3)

$$VP_{\text{pav zone}} = VB_{\text{pav zone}} \times \emptyset$$
(3)

- 4. The displaced water volume was measured as  $895 \text{ cm}^3$ , and after adjusting for the internal volume of one pipe ( $V_{w, adjusted}$ ) was  $893 \text{ cm}^3$ .
- 5. Connate Water Saturation (Swc) was determined using Eq. (4)

$$S_{wc} = \frac{VP_{pay\ zone} - V_{w,adjusted}}{VP_{pay\ zone}} = \frac{1041 - 893}{1041} = 14.3\%$$
 (4)

6. The initial oil saturation ( $S_{0i}$ ) was calculated to equal 85.7% from the material balance as follows in Eq. (5)

$$S_{oi} = 1 - S_{wc} \tag{5}$$

7. After determining S<sub>wc</sub>, n-decane was injected at a constant rate from the top valve, and production was recorded from the horizontal well. The injection was driven by a constant head system, utilizing a floating valve and graduated beaker to maintain a stable pressure differential, similar to the procedure for absolute permeability measurement. The injection pressure was monitored using the pressure gauge installed on the n-Decane injection line (refer to section 2.4), while the outlet pressure at the production



well was atmospheric. The flow rate of n-Decane was monitored using the flowmeter. The following parameters were used for effective oil permeability ( $K_{0e}$ ) calculations: the viscosity of n-decane was 0.84 cP at room temperature, the flow path length was 32.5 cm, the cross-sectional area was 92.1 cm<sup>2</sup>, and the pressure drop and flow rate were experimentally recorded as 0.0888 atm and 1.25 cm<sup>3</sup>/s, respectively. The effective oil permeability was calculated using Darcy's equation, Eq. (6), to be 4.2 Darcy.

$$K_{oe} = \frac{Q \times \mu \times L}{A \times \Delta P} \tag{6}$$

8. The relative permeability of n-Decane at Swc ( $K_{roe}$ ) was calculated to be 0.84, using Eq. (7)

$$K_{\text{roe}} = \frac{K_{\text{oe}}}{K_{\text{abs.}}} \tag{7}$$

The model and pay zone characteristics are summarized in **Table 3**.

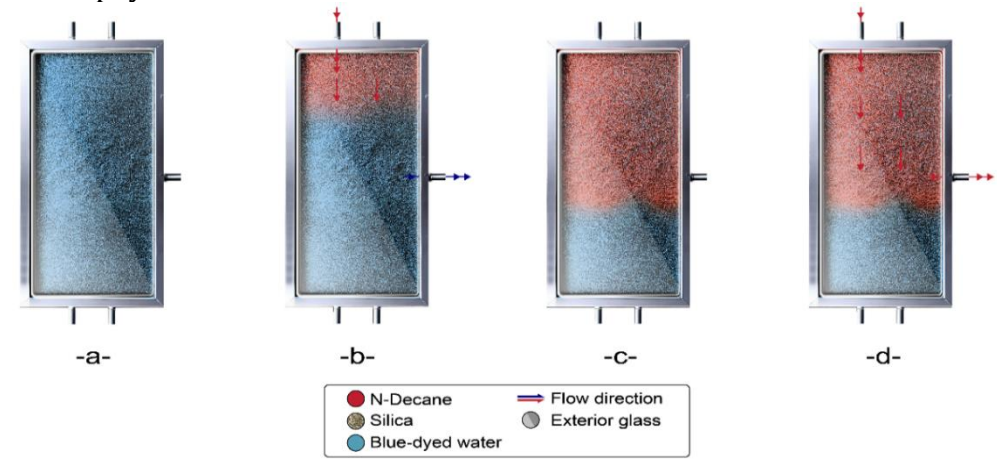


**Figure 6.** Fluid saturation and permeability parameters measurement procedure: (a) Hele-Shaw model fully saturated with water. (b) Injecting n-Decane via top valve to displace water through the horizontal well. (c) Displacement stops when the OWC is established. (d) Effective permeability measurement with constant n-Decane flow rate.

**Table 3.** Model description and measured characteristics of the pay zone.

Parameter	Value	Remarks
Model Dimensions (L × W × H), cm	30.7 × 3 ×	Overall dimensions of the experimental model.
	60	
Pay Zone Thickness, cm	35	Height of the pay zone saturated with oil.
Distance (OWC→ Bottom), cm	25	Represents the water aquifer in the reservoir.
Distance (Bottom → Horizontal Well), cm	27.5	Location of the horizontal well in the model.
Cross-sectional Area (A), cm <sup>2</sup>	92.1	Calculated as the area available for flow.
Model Bulk Volume (Silica), cm <sup>3</sup>	5440	Total volume accounting for pipes and fittings.
Pore Volume of Total Model, cm <sup>3</sup>	1,771	Adjusted water volume saturating the model.
Porosity (φ) %	32.5	Based on adjusted water volume in silica pack.
Absolute Permeability, Darcy	5.02	Based on experimental trendline
Pore Volume (Pay Zone), cm <sup>3</sup>	1041	Calculated using adjusted water volume and porosity.



Adjusted Displaced Water Volume, cm <sup>3</sup>	893	Volume of water displaced during the experiment
Connate Water Saturation (swc) %	14.3	Fraction of the pore volume is occupied by water.
Initial Oil Saturation (Soi) %	85.7	Fraction of the pore volume occupied by oil.
OOIP, cm <sup>3</sup>	893	Volume of Oil Initially in Place, cm <sup>3</sup>
K <sub>oe</sub> @ S <sub>wc</sub> , D	4.761	Effective Permeability to Oil at Swc

#### 3. MODEL RESET AND NEXT RUN PREPARATION

To ensure repeatability across multiple experiments, the model must be prepared for the next run by establishing its new initial conditions following each run. The model undergoes water flooding by injecting water from bottom valves, initially produced from the horizontal well, followed by production from top valves. The volume of oil displaced throughout this procedure is collected and recorded. The model must be thoroughly flushed before resaturation with n-Decane. The new OOIP,  $S_{0i}$ , and  $S_{wc}$  were calculated, setting the initial conditions for the next run. The procedure for backwashing and the calculations related to model preparation are summarized in **Fig. 7**.

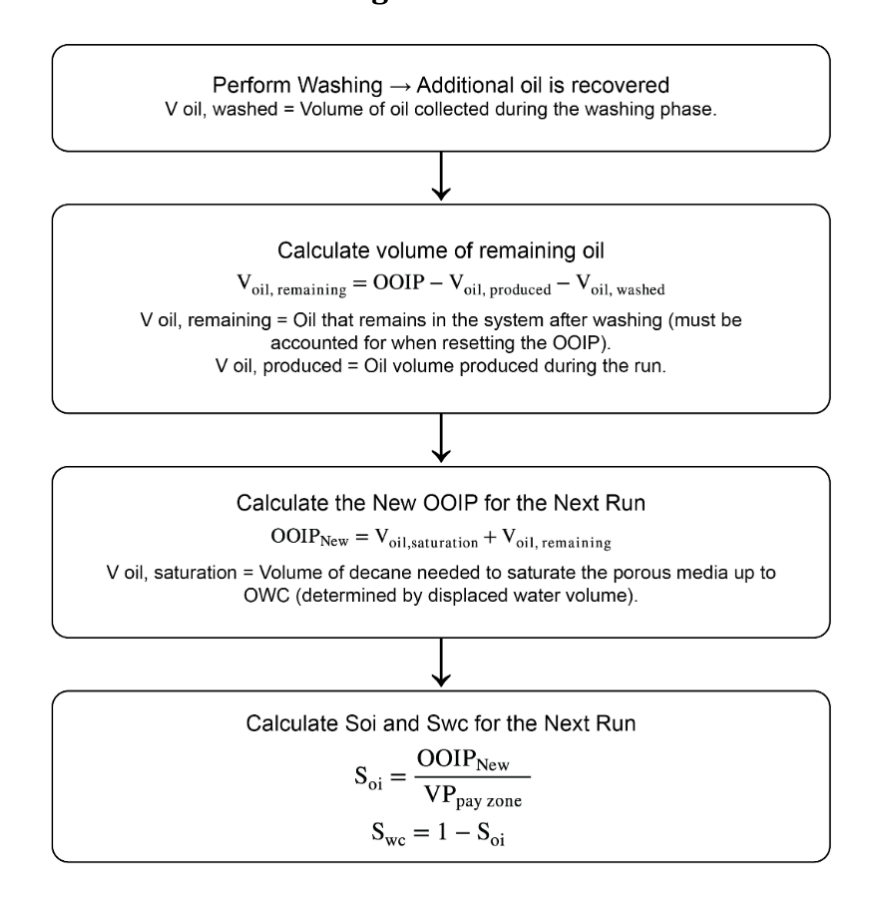


**Figure 7.** Experimental workflow to determine the new OOIP, Soi, and Swc parameters.

#### 4. RESULTS AND DISCUSSION

A series of experiments, listed as FFGD1, FFGD2, and FFGD3 in **Table 4**, were designed to investigate the combination-drive mechanism of FFGD supported by a water drive, and to evaluate how varying water-drive strengths influence oil recovery and water cutting. The runs were performed under a restricted production rate (50% valve opening) while maintaining all other parameters constant except for aquifer pressure. Each experiment



lasted 240 minutes, with oil recovery and water cut monitored continuously. Observations focused on oil bank advancement, water cresting behavior, and the movement of the OWC.

**Table 4.** The processing variables and the experimental runs.

Run	Water-drive Pressure (psig)
FFGD1	1.15
FFGD2	0.94
FFGD3	0.725

**Fig. 8** illustrates the recovery trends for the three experimental runs, highlighting the evolution of production behavior in response to varying water-drive strengths, with several key observations: FFGD1, with the strongest water-drive support (1.15 psig), exhibited a rapid initial oil recovery, recovering approximately 75% of OOIP within the first 60 minutes. FFGD2 (0.94 psig) demonstrated lower oil production and longer recovery buildup, achieving about 65% of OOIP at 60 minutes. FFGD3, conducted with the weakest water-drive support (0.725 psig), showed the lowest recovery performance among the runs, recovering approximately 55% of OOIP after 60 minutes, and continued with a lower recovery rate over the 240-minute run.

A comparison of ultimate recoveries indicates that FFGD1 achieved its ultimate recovery (~79.5% of OOIP) within approximately 120 minutes, after which oil production largely plateaued. FFGD2 achieved its ultimate recovery of approximately 77.2% after around 200 minutes, after which it stabilized. FFGD3 resulted in an even lower ultimate recovery of about 70.2% and exhibited a steady, gradual recovery trend throughout the experiment, without reaching a clear plateau. These findings highlight that a stronger water drive promotes a higher recovery rate and ultimately higher recovery.

The impact of aquifer strength is further highlighted in the water cut trends illustrated in **Fig. 9**. In FFGD1, water broke through rapidly after approximately 2.5 minutes, with water cut exceeding 90% within the first hour. In FFGD2, a breakthrough occurred around 4.5 minutes, after which the water cut increased gradually, remaining below 80% until about 150 minutes. Notably, FFGD3 produced no water throughout the experiment.

The comparatively lower water cut trend observed in FFGD2 can be explained by its moderate water-drive pressure (0.94 psig). Consequently, water crest advancement was more controlled in FFGD2 than in FFGD1, thereby delaying excessive water production and reducing water handling challenges throughout the run. In FFGD3, the applied water-drive pressure of 0.725 psig was only sufficient to maintain the OWC at a stable position near 25 cm from the model base, but insufficient to push the water crest above the horizontal production well, which was placed at 27.5 cm. In this run, the water level in the beaker feeding the aquifer was set approximately at the same elevation as the OWC, consistent with maintaining rather than advancing the water front. As a result, the water front stabilized below the well perforations throughout the experiment. This operational arrangement explains the observed zero water cut in FFGD3, highlighting how a weak aquifer drive can maintain reservoir pressure without causing water production, which sustains oil production while avoiding water handling challenges. A summary of key experimental results, including the differences in recovery factor, water cut, and residual oil, is presented in **Table 5**.



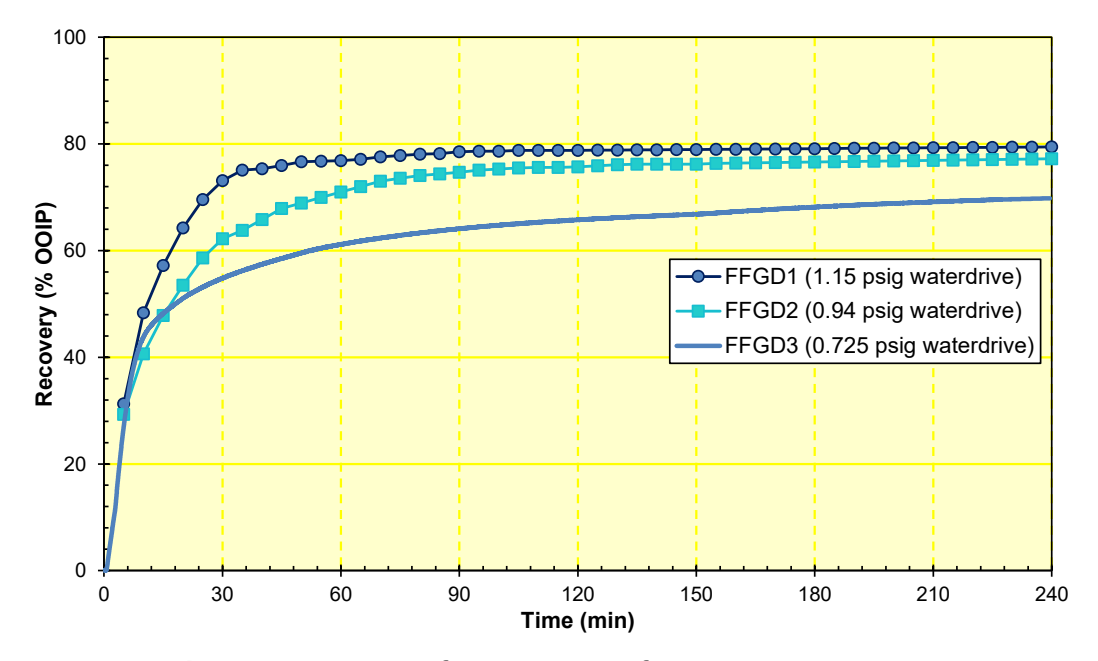
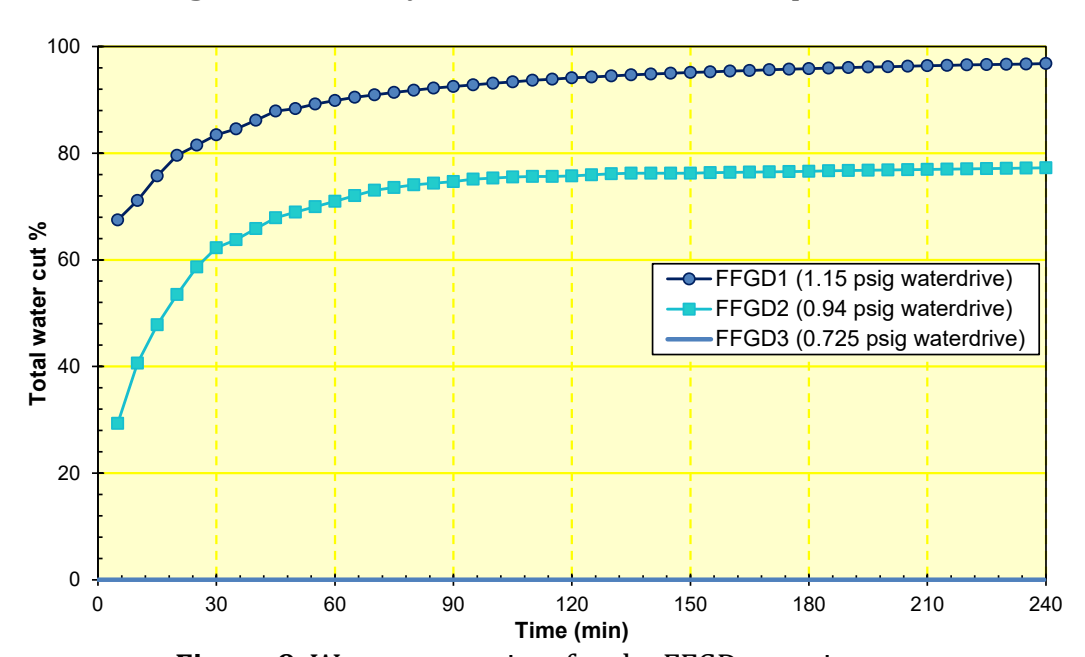


Figure 8. Recovery factor vs. time for FFGD experiments.



**Figure 9.** Water cut vs. time for the FFGD experiments.

**Table 5.** Summary of the experimental results.

Experiment	PV	OOIP	Soi	Swc	Sor	Ultimate Oil	Final Water
	(cm <sup>3</sup> )	(cm <sup>3</sup> )	(%)	(%)	(%)	Recovery (%)	<b>Cut (%)</b>
FFGD1	1041	848	81.5	18.5	16.8	79.5	96.8
FFGD2	1041	972	93.3	6.7	21.3	77.2	91.9
FFGD3	1041	975.6	93.7	6.3	27.9	70.2	0

Since the same fluid system was used across the runs, the mobility ratios remained constant across experiments and did not act as a controlling variable. Therefore, the observed variations in recovery efficiency and front stability are attributed primarily to differences in water-drive strength.



**Figs. 10** and **11** show the sequence of displacements that took place over the FFGD runs under the strongest (FFGD1) and weakest (FFGD3) aquifer supports, respectively. Initially, the 35 cm oil column established within the model created a gravitational potential equivalent to 0.36 psig, serving as the primary driving force for oil drainage before the water drive became active. In both scenarios, the first 30 minutes of production were characterized by rapid advancement of the oil bank due to the initially high hydrostatic pressure. However, due to its weaker aquifer support, FFGD3 exhibited a relatively slower oil bank progression in this initial phase than FFGD1. Beyond the first 30 minutes, as the hydrostatic pressure from the oil column declined with production, the influence of aquifer support became more dominant in governing displacement behavior and recovery rate.

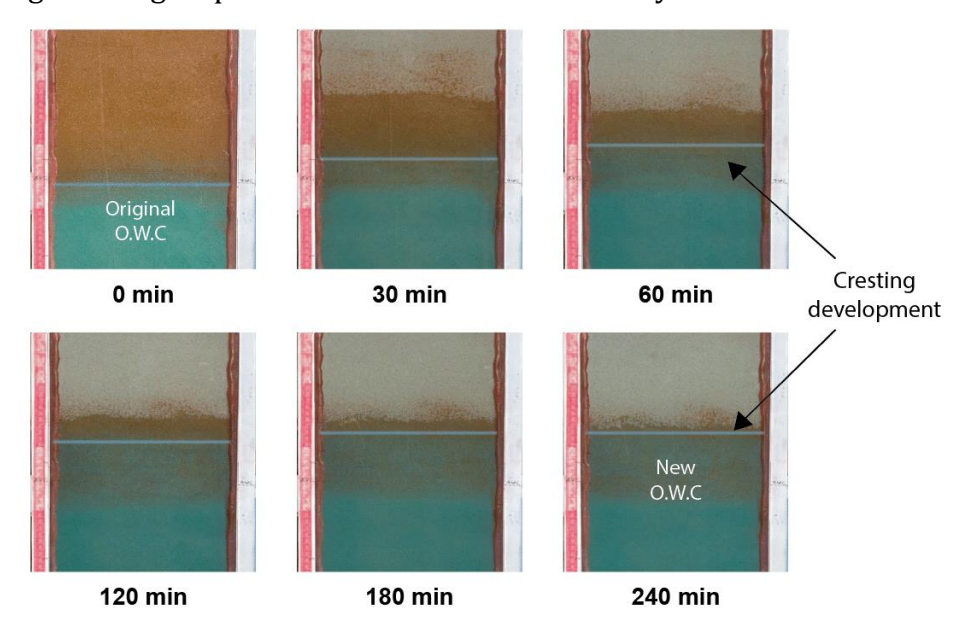


**Figure 10.** Time-sequence images showing oil bank advancement and water cresting behavior in the FFGD1 under the strongest aquifer support.

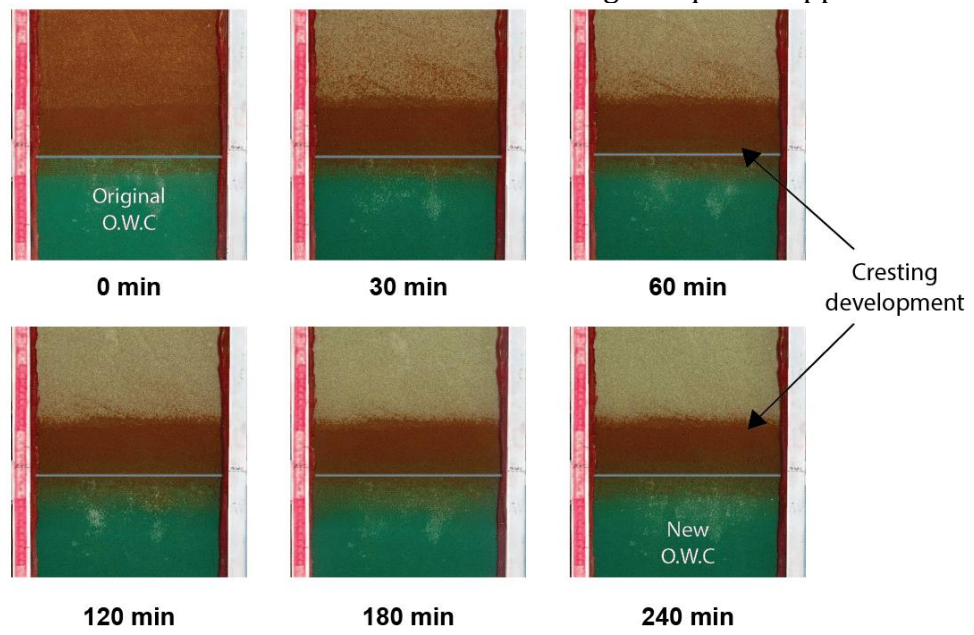


**Figure 11**. Time-sequence images showing the oil bank advancement and water cresting behaviour in the FFGD3 under the weakest aquifer support.



In FFGD1, the rapid initial production was accompanied by significant early water cresting that developed vertically and stabilized after about 180 minutes, with an elevated new OWC by the end of the run, driven by the strong aquifer support. In contrast, FFGD3 showed limited cresting, with only minor upward movement of the OWC over the 240-minute run. The amount of this residual oil was higher in FFGD3 than in FFGD1, which can be attributed to the reduction in gravity potential as the oil column declined with production, combined with the limited support from the aquifer. These conditions limited the driving force for oil displacement and left a higher residual oil. The faint brown color consistently visible below the OWC in both experiments represents residual oil that was not fully mobilized by the water front, where bypassed oil blobs can remain disconnected due to capillary forces, with only limited remobilization occurring over time.

## 5. IMPACT OF POROUS MEDIUM HETROGENITY: COMPARISON WITH LITERATURE

This study also aimed to investigate the influence of reservoir heterogeneity on FFGD performance by comparing its results with those from a previous experimental investigation performed in a heterogeneous porous medium (Al-Obaidi, 2020). Both studies employed comparable Hele-Shaw-type apparatuses and similar fluid systems (n-Decane and deionized water), providing a consistent basis for isolating the impact of porous medium heterogeneity on the FFGD mechanism. One dataset was extracted from the previous study's FFGD run (Ref-FFGD). The key differences in porous medium characteristics between the two models are summarized in **Table 6**, highlighting distinctions in packing, particle size, porosity, and permeability.

Parameter	Homogeneous system	Heterogeneous system	
Porous Medium	Ottawa Silica Sand, D50 = 0.84 mm	Pure silica; 3 graded size ranges mixed	
Packing Technique	Uniform dry packing with fine sand only	Layered packing: coarse sand used top/bottom, fine in the middle	
Median Particle Size (mm)	0.84 (homogeneous grain size)	Mixed: 0.126-0.141, 0.251-0.282, 0.600- 0.840	
Porosity (%)	32.5	24.5	
Permeability (D)	5.02	1.940	

**Table 6.** Key differences between the two experimental systems.

To ensure a reasonable comparison, an additional run (FFGD4) was conducted for 300 minutes under the same aquifer pressure and production conditions as the Ref-FFGD, with a water drive of 0.85 psig and full production conditions (100% valve opening), allowing reservoir heterogeneity to be isolated as the key variable. **Fig. 12** shows the recovery trend of FFGD4. The findings highlight a notable difference in performance between the two systems. FFGD4 achieved a final oil recovery of 79% with no observed water production during the 300-minute run. Ref-FFGD recovered only 61.58% and experienced early water breakthrough after just 5 minutes, resulting in a final water cut of 81%. The absence of water production in the homogeneous system suggests that the water crest developed uniformly and progressed steadily, without forming preferential flow paths toward the production well. **Fig. 13** shows time-sequence images of the run. In contrast, the early water breakthrough observed in Ref-FFGD implies that heterogeneities, such as high-permeability streaks, facilitate water encroachment toward the production well. Such heterogeneity can



promote channeling, where water preferentially follows the most permeable paths, bypassing oil-rich zones. Furthermore, in the Ref-FFGD run, the oil bank reached production well after 25 minutes, with a substantial amount of residual oil left behind. In FFGD4, the oil bank was not produced within the 300-minute run, indicating a more stable and slower advancement rate with improved sweep efficiency. **Table 7** summarizes the key performance indicators for both cases. This comparison demonstrates the significant challenge imposed by reservoir heterogeneity **(Tan et al., 2022)**.

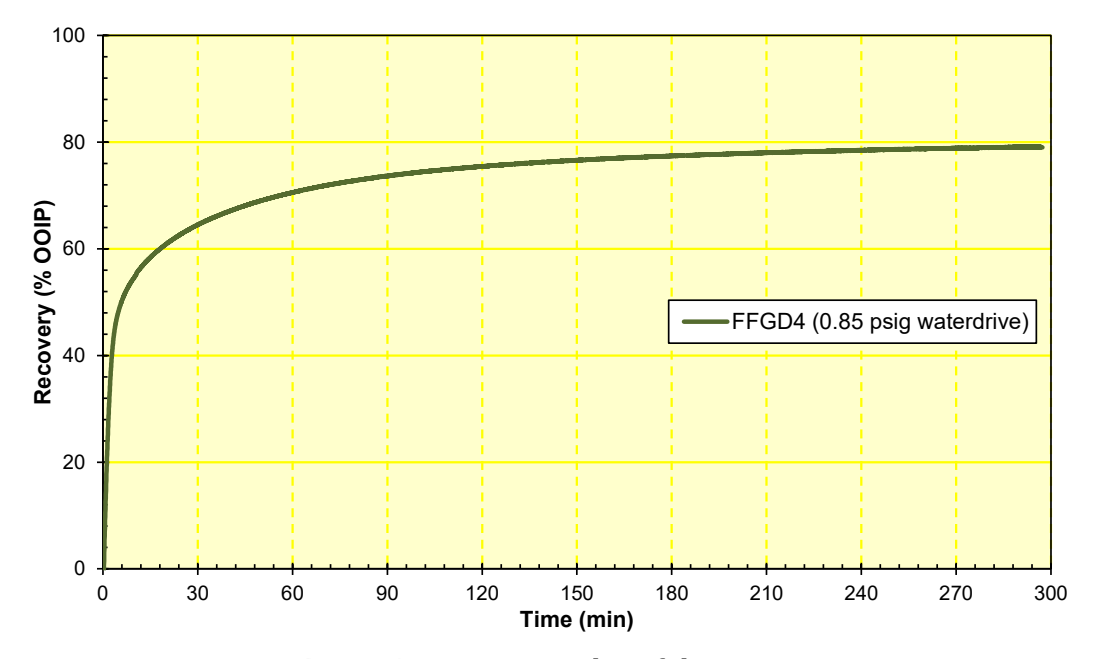


**Figure 12.** Recovery plot of the FFGD4.

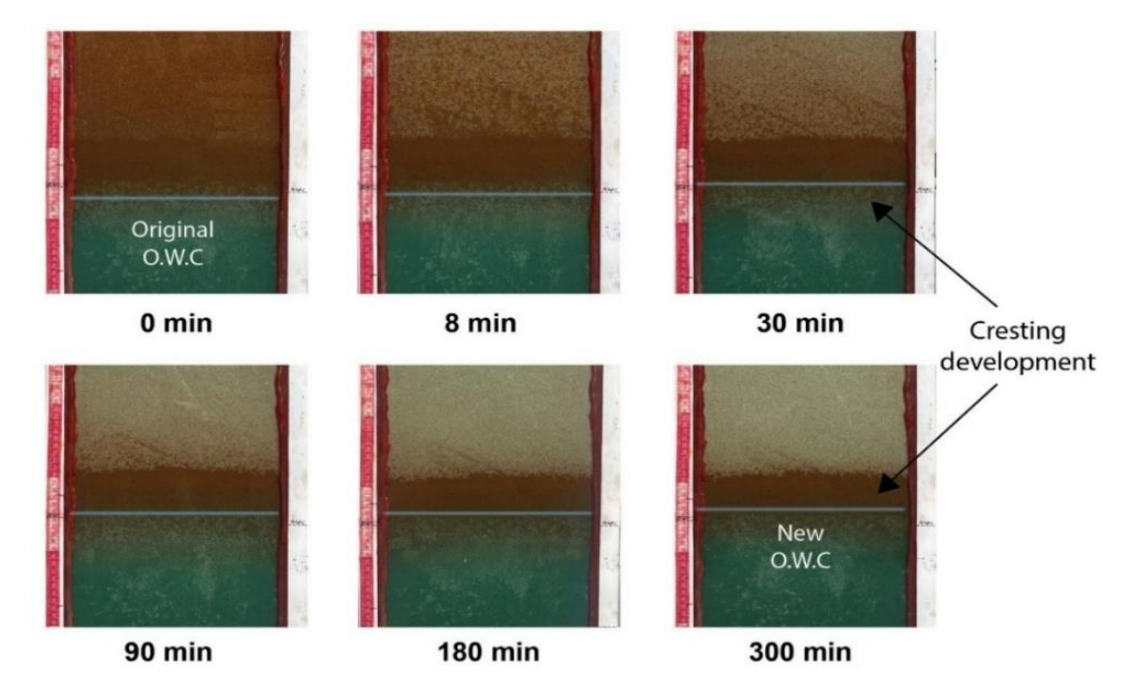


**Figure 13.** Time-sequence images of the FFGD4 showing oil bank advancement and limited water cresting in the homogeneous porous medium.



**Table 7.** Key Performance Indicators for FFGD in Homogeneous and Heterogeneous Systems.

Parameter	FFGD4	Ref-FFGD (FFGD2)
Reservoir Type	Homogeneous	Heterogeneous
Aquifer Pressure (psig)	0.85	0.85
Gas Injection	No Gas	No Gas
Total Oil in Model (cc)	904	617
Ultimate Oil Recovery (%)	79	61.58
Final Water Cut (%)	0	81
Onset of Water Production (min)	Not observed (300)	~5
Frontal Arrival at Production Well (min)	Not observed (300)	~25

#### 6. CONCLUSIONS

This study aimed to evaluate the performance of the FFGD process in a water-drive reservoir using a 2D visual Hele-Shaw model. The work focused on understanding how bottom-water drive strength and porous medium heterogeneity affect oil recovery, fluid front behavior, and water handling. A total of four FFGD experiments were conducted using bottom-water drive under constant pressure. The experimental setup emphasized visual tracking of fluid movement and the influence of parameters under investigation. Based on the experimental findings and analysis, the following conclusions are drawn:

- 1. An initial 35 cm oil column established a gravitational driving force of approximately 0.36 psig, enabling rapid early free-fall gravity drainage before the water drive became dominant. This initial gravity-driven stage was evident in the comparable early oil bank advancement across all experiments during the first 30 minutes of production.
- 2. The influence of water-drive strength was critical in shaping FFGD performance. A stronger water drive promoted higher early production rates and ultimate recovery, with aquifer pressure of 1.15 psig in FFGD1 accelerating recovery to ~75% of OOIP within 60 minutes and achieving 79.5% ultimate recovery in 120 minutes. Moderate and weak water drives (0.94 and 0.725 psig) resulted in ultimate recoveries of 77.2% and 70.2%, respectively.
- 3. Water cresting behavior varies significantly with water-drive strength. FFGD1 experienced a rapid water breakthrough after 2.5 minutes, resulting in water cuts above 90% early on, whereas the weakest drive in FFGD3 maintained a stable OWC with no water production over 240 minutes, thereby minimizing water handling requirements.
- 4. Visual tracking of cresting and OWC movement indicated that stronger water drives promoted vertical water crest development and elevated the OWC over time, while a weaker water drive stabilized the OWC below the perforations. This stabilization preserved the oil bank and extended the gravity drainage period, reflecting a better balance between pressure support and water production challenges.
- 5. Residual oil saturation was higher under weaker aquifer conditions, reaching 27.9% in FFGD3 versus 16.8% in FFGD1. This is attributed to the reduction in gravity potential as the oil column is depleted with production and limited water drive. These conditions limit the driving force for oil displacement, resulting in a higher residual oil.
- 6. The analysis of heterogeneity's impact on FFGD performance in a water-drive reservoir indicated that homogeneity notably enhanced oil recovery and water management, resulting in an ultimate recovery of 79.0%, with no water production throughout the 300-minute run. The heterogeneous system recovered 61.58%, with water production



- occurring approximately 5 minutes after the start of the run and a final water cut of 81%, highlighting the impact of reservoir heterogeneity on early water encroachment and sweep efficiency.
- 7. The heterogeneous system facilitates preferential flow pathways, as seen in the Ref-FFGD case, where rapid water encroachment led to early water breakthrough and left significant residual oil behind. In Ref-FFGD, the oil bank reached the production well after just 25 minutes, in contrast to the homogeneous medium (FFGD4), which supported a stable water crest and delayed the oil bank's arrival beyond 300 minutes, thereby improving sweep efficiency and overall recovery.

#### **NOMENCLATURE**

Symbol	Description	Symbol	Description
Α	Cross-sectional area, cm <sup>2</sup>	Swc	Connate water saturation, %
$D_p$	Grain diameter, mm	T	Time, s
Н	Pay zone height, cm	VB	Bulk volume, cm <sup>3</sup>
K	Absolute permeability, Darcy	VP	Pore volume, cm <sup>3</sup>
Koe	Effective permeability to oil,	α	Inclination angle (not explicitly used),
	Darcy		deg
Kroe	Relative permeability to oil at	β	Correction/variation factor (general
	Swc, dimensionless		symbol), dimensionless
L	Flow path length, cm	μ	Fluid viscosity, cP
OOIP	Original oil in place, cm <sup>3</sup>	ф	Porosity, fraction
Q	Volumetric flow rate, cm <sup>3</sup> /s	τ	Tortuosity, dimensionless
Sorg	Residual oil saturation, %	ΔΡ	Pressure drop, atm
Soi	Initial oil saturation, %		

#### **Acknowledgements**

This work was supported by the Petroleum Engineering Department, College of Engineering, University of Baghdad.

## **Credit Authorship Contribution Statement**

Rufaida T. Ibrahim: Conceptualization, Methodology, Investigation, Writing – Original Draft, Data Curation. Dahlia A. Alobaidi: Supervision, Writing – Review & Editing, Validation. Watheq J. Al-Mudhafar: Writing, Review & Editing. Dandina N. Rao: Writing, Review & Editing

# **Declaration of Competing Interest**

The authors declare that they have no known competing financial interests or personal relationships that could have appeared to influence the work reported in this paper.

#### **REFERENCES**

Abdulrahman, A.A.A., 2019. An experimental study of fractional wettability effects on gas assisted gravity drainage (GAGD). MSc thesis, Craft & Hawkins Department of Petroleum Engineering, Louisiana State University and Agricultural and Mechanical College, USA.

Ahmed, T., 2019. Reservoir engineering handbook. 5th ed. Elsevier. ISBN: 9780128136492.



Ahmed, T., McKinney, P.D., 2004. *Advanced reservoir engineering*. 1st ed. Oxford: Gulf Professional Publishing. ISBN: 978-0-7506-7733-2.

Alamooti, A.M. and Malekabadi, F.K., 2018. An introduction to enhanced oil recovery. *Fundamentals of enhanced oil and gas recovery from conventional and unconventional reservoirs*, pp. 1-40. https://doi.org/10.1016/B978-0-12-813027-8.00001-1.

Al-Mudhafar, W.J., Rao, D.N., Srinivasan, S., 2018. Robust optimization of cyclic CO<sub>2</sub> flooding through the gas-assisted gravity drainage process under geological uncertainties. *Journal of Petroleum Science and Engineering*, 166, pp. 490–509. https://doi.org/10.1016/j.petrol.2018.03.044.

Al-Obaidi, D., 2020. Feasibility of water sink-based gas flooding to enhance oil recovery in North Rumaila oil field. PhD thesis, Department of Petroleum Engineering, University of Baghdad, Iraq.

Al-Obaidi, D.A., Al-Jawad, M.S., 2020. Numerical simulation of immiscible  $CO_2$ -assisted gravity drainage process to enhance oil recovery. *Iraqi Journal of Science*, 61(8), pp. 2004–2016. https://doi.org/10.24996/ijs.2020.61.8.17.

Al-Obaidi, D.A., Al-Mudhafar, W.J., Al-Jawad, M.S., 2022. Experimental evaluation of carbon dioxide-assisted gravity drainage process ( $CO_2$ -AGD) to improve oil recovery in reservoirs with strong water drive. *Fuel*, 324. https://doi.org/10.1016/j.fuel.2022.124409.

Al-Obaidi, D.A., Al-Mudhafar, W.J., Al-Jawad, M.S., 2024. Experimental influence assessments of water drive and gas breakthrough through the CO<sub>2</sub>-assisted gravity drainage process in reservoirs with strong aquifers. *Fuel*, 370. https://doi.org/10.1016/j.fuel.2024.131873.

Dumore, J.M., Schols, R.S., 1974. Drainage capillary-pressure functions and the influence of connate water. *Soc Pet Eng AIME J*, 14(5), pp. 437–444. https://doi.org/10.2118/4096-pa.

Dykstra, H., 1978. The prediction of oil recovery by gravity drainage. *Journal of Petroleum Technology*, 30(05), pp. 818–830. https://doi.org/10.2118/6548-PA.

Dzulkarnain, I., 2018. Investigation of flow mechanisms in gas-assisted gravity drainage process. PhD thesis, Department of Petroleum Engineering, Louisiana State University, USA.

Erfani, H., Rasouli, V., Aminian, K., Smith, J.E., 2021. Experimental and modelling study of gravity drainage in a three-block system. *Transport in Porous Media*, 136(2), pp. 471–494. https://doi.org/10.1007/s11242-020-01521-x.

Ezeaneche, O.S., Onyia, C.A., Enweremadu, C.C., Udeh, N.E., 2021. Gravity drainage system: investigation and field development using geological modelling and reservoir simulation. *SPE Nigeria Annual International Conference and Exhibition* 2021. https://doi.org/10.2118/207117-MS.

Hagoort, J., 1980. Oil recovery by gravity drainage. *Society of Petroleum Engineers Journal*, *20*(03), pp. 139-150. https://doi.org/10.2118/7424-PA.

Hasanzadeh, M., Jamialahmadi, M., Müller-Steinhagen, H., 2021a. New insights into forced and free fall gravity drainage performance in a fractured physical model. *Journal of Petroleum Science and Engineering*, 203. https://doi.org/10.1016/j.petrol.2021.108568.

Jadhawar, P.S. and Sarma, H.K., 2012. Effect of well pattern and injection well type on the CO2-assisted gravity drainage enhanced oil recovery. *Journal of Petroleum Science and Engineering*, 98, pp. 83-94. https://doi.org/10.1016/j.petrol.2012.09.004.



Joshi, S.D., 1991. *Horizontal well technology*. Tulsa, OK: PennWell Publishing Company. ISBN: 9780878143504.

Lewis, J.O., 1942. Gravity drainage in oil fields. *Transactions of the AIME*, 155(1), pp. 133–146. https://doi.org/10.2118/944133-G.

Mahmoud, T.N. and Rao, D.N., 2007, November. Mechanisms and performance demonstration of the gas-assisted gravity-drainage process using visual models. In *SPE Annual Technical Conference and Exhibition*, pp. SPE-110132. SPE. https://doi.org/10.2118/110132-MS.

Mahmoud, T.N. and Rao, D.N., 2008. Range of operability of gas-assisted gravity drainage process. In *SPE Improved Oil Recovery Conference*, pp. SPE-113474. SPE. https://doi.org/10.2118/113474-MS.

Mello, S.F. de, Trevisan, O.V., Schiozer, D.J., 2009. Review on gravity drainage performance. In: *Proceedings of the 20th International Congress of Mechanical Engineering (COBEM 2009)*, November 15–20, Gramado, RS, Brazil.

Moghaddam, M.B., Rasaei, M.R., 2015. Experimental study of the fracture and matrix effects on free-fall gravity drainage with micromodels. *SPE Journal*, 20(02), pp. 324–336. https://doi.org/10.2118/171555-PA.

Muskat, M., 1949. *Physical principles of oil production*. McGraw-Hill Book Co. ISBN: 978-0-934634-07-6.

Oliviera, I.B., Demond, A.H., Salehzadeh, A., 1996. Packing of sands for the production of homogeneous porous media. *Soil Science Society of America Journal*, 60(1), pp. 49–53. https://doi.org/10.2136/SSSAJ1996.03615995006000010010X.

Rao, D.N., Girard, M., Lee, J.I., 2004. Development of gas-assisted gravity drainage (GAGD) process for improved light oil recovery. *SPE Annual Technical Conference*.

Rao, D.N., Ayirala, S.C., Kulkarni, M.M. and Sharma, A.P., 2004, April. Development of gas assisted gravity drainage (GAGD) process for improved light oil recovery. In *SPE Improved Oil Recovery Conference?* pp. SPE-89357. SPE. https://doi.org/10.2118/89357-MS.

Rao, D.N., 2012. Gas-assisted gravity drainage (GAGD) process for improved oil recovery. U.S. Patent 8,215,392 B2, issued July 10, 2012. https://patents.google.com/patent/US8215392B2/en

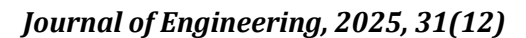
Ren, W., Bentsen, R.G. and Cunha, L.B., 2005. A study of the gravity assisted tertiary gas injection processes. *Journal of Canadian Petroleum Technology*, 44(02). https://doi.org/10.2118/05-02-02.

Rostami, B., Ayatollahi, S., Rashidi, F., 2010. Gas-oil relative permeability and residual oil saturation as related to displacement instability and dimensionless numbers. *Oil and Gas Science and Technology*, 65(2), pp. 299–313. https://doi.org/10.2516/ogst/2009038.

Ruiz Paidin, W., 2006. Physical model study of the effects of wettability and fractures on gas assisted gravity drainage (GAGD) performance. MSc thesis, Department of Petroleum Engineering, Louisiana State University, USA.

Schechter, D.S. and Guo, B., 1996, March. Mathematical modeling of gravity drainage after gas injection into fractured reservoirs. In *SPE Permian Basin Oil and Gas Recovery Conference*, pp. SPE-35170. SPE. https://doi.org/10.2118/35170-MS

# R. T. Ibrahim et al.





Sharma, A.P., 2005. Physical model experiments of the gas-assisted gravity drainage process. MSc thesis, Department of Petroleum Engineering, Louisiana State University and Agricultural and Mechanical College, USA.

Sharma, A.P., Rao, D.N., 2008. Scaled physical model experiments to characterize the gas-assisted gravity drainage EOR process. *In Proceedings of the 2008 SPE/DOE Improved Oil Recovery Symposium. Tulsa, OK, USA*, pp. 773–795. https://doi.org/10.2118/113424-MS.



# التقييم التجريبي لعملية التصريف بالجاذبية الحرة في المكامن ذات الدفع المائي: تأثير قوة التقييم الدفع المائي وتجانس/عدم تجانس الطبقة المكمنية

رفيده ثامر ابراهيم $^{1,*}$ ، دانيا عبدالهادي العبيدي $^{1}$ ، واثق جاسم المظفر  $^{2}$  ، داندينا راو  $^{8}$ 

أقسم هندسة النفط، كلية الهندسة، جامعة بغداد، بغداد، العراق شركة نفط البصرة، البصرة، العراق أجامعة لويزيانا، الولايات المتحدة الاميركية

#### الخلاصة

بحثت هذه الدراسة تجريبيًا في التصريف بالجاذبية الحرة (FFGD) تحت ظروف الدفع المزدوج باستخدام نموذج هيلي—شو ثنائي الأبعاد يحاكي مكمنًا يعمل بالدفع المائي. مكنت قوة الجاذبية العالية في بداية التشغيل من عمود النفط على تسريع تصريف النفط خلال المرحلة الأولى قبل ان يصبح دور الدفع المائي هو السائد. تمت دراسة ثلاث درجات من قوة الدفع المائي، حيث أظهر الدفع الأقوى (1.15 رطل/بوصة²) قدرة على تسريع الاستخلاص إلى نحو 75% من النفط الأصلي في المكمن (OOIP) خلال 60 دقيقة، مع تحقيق نسبة استخلاص نهائية بلغت 79.5%, رغم ملاحظة اختراق مبكر الماء بعد 2.5 دقيقة وارتفاع نسبة انتاج الماء لأكثر من 90%. في المقابل، أدى الدفع المائي الأضعف (70.75 رطل/بوصة²) إلى تثبيت التماس بين النفط والماء (OWC) وتأخير وصول الماء إلى البئر، مع الحفاظ على نسبة انتاج ماء 0 طوال 240 دقيقة، وإن كانت نسبة الاستخلاص النهائي أقل وبلغت 70.2%. أكدت الملاحظات البصرية أنه تم الحفاظ على تقدم مائي مستقر وجبهة النفط لفترة أطول تحت ضغوط الدفع المائي المعتدلة إلى الضعيفة، مما أطال فترة الاستخلاص المسيطر عليه بالجاذبية وساهم في تقليل متطلبات إدارة المياه المنتجة. كان تشبع النفط المتبقي أعلى في ظل الدفع المائي الأضعف (27.9%) مقارنة بالدفع الأقوى وسط مسامي غير متجانس انخفاضًا بنحو 22% في الاستخلاص النهائي، مع اختراق مبكر للماء خلال 5 دقائق، وذلك بسبب تعزيز التباين الطبقي لمسارات التدفق التقضيلي وسرعة وصول الماء إلى البئر، بينما حقق الوسط المتجانس إنتاجًا مستقرًا دون تعريز التباين الطبقي لمسارات التدفق النقضيلي وتعميق الفهم لآليات الاستخلاص المسيطر عليها بالجاذبية تحت ظروف اندع ماء طوال 300 دقيقة. تسهم هذه النتأتج في تعميق الفهم لآليات الاستخلاص المسيطر عليها بالجاذبية تحت ظروف

الكلمات المفتاحية: التصريف بالجاذبية الحرة (FFGD)، الدفع المزدوج، قوة الدفع المائي، كفاءة استخلاص النفط، نموذج هيلي-شو.